Formation of Delta-Ferrite in the Weld Metal of 9-12Cr Steels

K. V. Sajunath, C. R. Das, S. K. Albert*, S. Raju and A. K. Bhaduri
Indira Gandhi Centre for Atomic Research, Kalpakkam 603102, India
*E-mail:shaju@igcar.gov.in

ABSTRACT

Formation of delta-ferrite in the weld metal, during autogenous bead-on-plate welding of 9-12Cr steels, using gas tungsten arc welding (GTAW) process has been studied. The microstructure of 9-12Cr steel base metal consists of tempered lath martensite, where precipitates decorate the boundaries. In single pass bead-on-plate, the area fraction of delta-ferrite was found to be higher at the weld interface as compared to center of the weld metal at all preheat temperatures. Decrease the area fraction of delta-ferrite, with an increase in preheat temperature were observed. Area fraction of delta-ferrite was found to be 7.6 in P91B weld metal at room temperature compared to that of 6.1 at preheat temperature of 250°C, whereas it was 5.7 in AISI 410 weld metal at room temperature and 3.9 at pre heat temperature of 250°C. High cooling rate caused stability of delta ferrite at room temperature as well as preheat condition in the weld metal.

Keywords: Weld metal, Cooling rate, Area fraction of delta-ferrite,

1.0 INTRODUCTION

9-12 Cr ferritic steels having good thermal conductivity, low thermal expansion coefficient, good high temperature mechanical properties, corrosion resistance, good formability and weldability are used in fossil power plants and steam generator of Fast Breeder Reactors [1-3]. Observation of the equilibrium phase diagram of the Fe-Cr-0.1%C reveals that the steel with 9-12 Cr exists in one of the several sub-liquidus phase fields depending on the temperature experienced. While cooling from austenetising temperature to room temperature, austenite phase transformed into martensite [4]. In order to achieve 100% martensite at room temperature, a careful balance between ferrite and austenite stabilising elements is required. From the equilibrium phase diagram it was also known that delta-ferrite may form in these steels if austenisation temperature is above 1200°C [4-6]. Hence, careful heat treatment procedure is required to avoid formation of delta-ferrite in these materials, as its presence at room temperature is unwarranted. Therefore, austenite stabilising elements are added in 9-12Cr steel in such a way that the formation of delta-ferrite during heat treatment does not take place.

In spite of achieving fully martensitic microstructure after standard heat treatment, these steels have some tendency to form delta-ferrite at the weld interface and in the weld metal during the welding [7]. It is often observed during single pass welding of these steel but occasionally during multi pass welding. Therefore, weld consumables of matching composition to the parent material shall be used to avoid delta-ferrite in the weld metal. Presence of delta-ferrite in these steels has been reported to have several detrimental effects on mechanical properties [8,9]. Thus it is important to avoid its formation during welding. Therefore, in order to understand its formation during single and multi pass welding, a systematic

study was undertaken. For the present study, boron-added modified 9Cr-1Mo steel and AISI 410 SS is used.

2.0 EXPERIMENT

Boron-added modified 9Cr-1Mo steel designated as P91B and AISI 410 SS of 250 x 500 x 12 mm^3 were received in the normalised (1050°C/30min) and tempered (760°C/3h) conditions. Differential scanning calorimetry (DSC) study was carried out only on P91B. Small specimen of P91B having Φ 3 mm diameter is used for DSC experiment. The rectangular plates of 150 x 125 x 10 mm^3 were cut from these plates. Autogenous bead-on-plate welding using gas tungsten arc welding process (GTAW), at a constant heat input of 1.1 KJ mm^{-1} was carried out at different preheat temperatures. Welding parameters are given in **Table 1**. Weld bead profile is shown schematically in **Fig. 1**.

Table 1 : Welding parameters used for bead-on-plate welding

Current (A)	Voltage (V)	Speed (mms^{-1})	Heat Input (KJ mm^{-1})
120	13	75	1.1

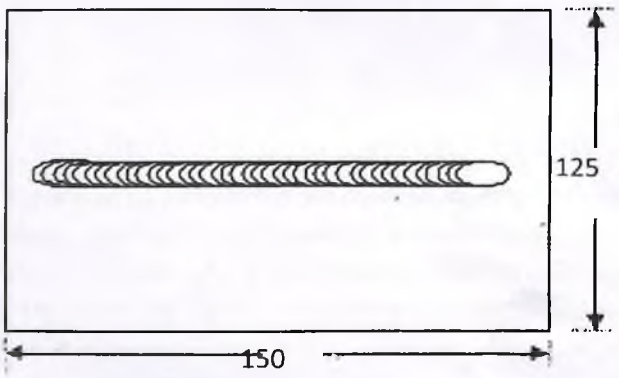

Figure 1 : Schematic diagram showings bead appearance on the plate

During welding the Tungsten-Rhenium (C-Type) thermocouple was plunged into the molten weld pool. The thermocouple was connected to the data logger, where the data logger acquires the data (temperature) for every 2 micro seconds. Cooling curves data were processed in order to find out stability of delta-ferrite in liquid phase as well as in austenite phase at high temperature. All bead-on-plate welds are subjected to post weld heat treatment (PWHT). It was 3 h at 760°C for P91B and 1h at 600°C for AISI 410 SS. Specimen of 15 x 5 x 10 mm^3 was cut from each bead-on-plate weldments and polished metallographically up to 0.25 μm using diamond slurry. Polished specimens were etched with Villella's reagent and observed under optical and Scanning Electron Microscope (SEM). For calculation of phase fraction image J software was used.

3.0 RESULTS

3.1 Chemical composition and microstructure of base metals

Chemical composition of these steels is given in **Table 2**. From the **Table 2**, it is evident that P91B contain 8.5 wt.% Cr, whereas AISI 410 SS contain 11.87 wt.% Cr. From the **Table 2**, it is also clear that P91B steel contains microalloying elements, like V and Nb and controlled amount of nitrogen. It is worth mentioning that nitrogen content was reduced to 20 ppm in P91B from 550-700 ppm specified in standard P91 steel.[10] This chemical composition adjustment was required to avoid formation of NB in P91B steel, which is known to be detrimental phase to the mechanical properties of boron-added ferritic steels [10].

Microstructure of as-received boron-added modified 9Cr-1Mo steel and AISI 410 SS is given in **Fig. 2(a,b)**. From **Fig. 2(a)**, it is evident that the microstructure of P91B consists of tempered lath martensite, where lath and prior austenite grain boundaries are decorated with precipitates.

Table 2 : Chemical composition of P91B and P91 steels

Elements	C	Cr	Mo	Si	Mn	V	Nb	S
P91B	0.1	8.5	1.04	0.40	0.3	0.23	0.09	0.002
410	0.098	11.87	-	0.46	0.82	-	-	0.005
Elements	P	Ni	Al	Ti	N	B	Cu	Fe
P91B	0.005	0.02	0.03	0.003	0.0021	0.0100	O.006	Bal.
410	0.011	0.11	-	-	-	-	-	Bal.

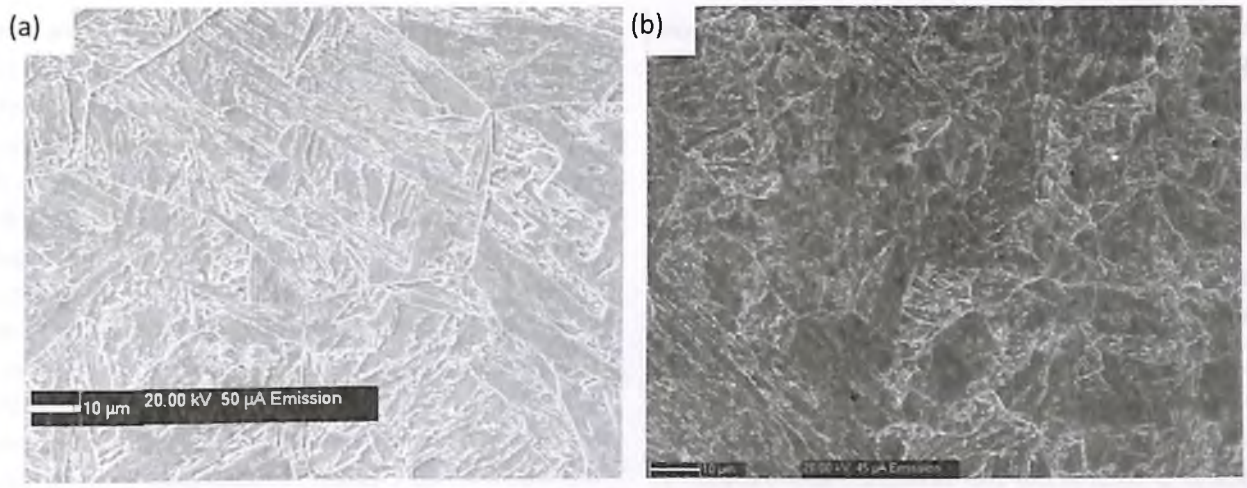

Figure 2 : Microstructure of (a) boron-added modified 9Cr-1Mo steel and (b) AISI 410 SS in normalised and tempered conditions.

These are $M_{23}C_6$ carbide precipitates enriched with Cr, Fe and Mo confirmed with EDS.[11] From **Fig. 2(a)** and **Fig. 2(b)** it is clear that prior austenite grain sizes are finer in 410 SS as compared to P91B and microstructure consists of tempered lath martensite, where precipitates decorate the boundaries.

3.2 Phase transformation during heating in P91 and P91B

In order to know the appropriate phase transformation temperatures, systematic DSC studies were carried out on P91B. **Fig. 3** is a DSC thermogram obtained for P91B during slow heating to a melting temperature followed by slow cooling to room temperature. Various phase transformations occurring during heating (A_{c1} and A_{c3} temperature) and cooling are shown in **Fig. 3** by arrows. The delta-ferrite formation starts at 1235°C according to the following reaction;

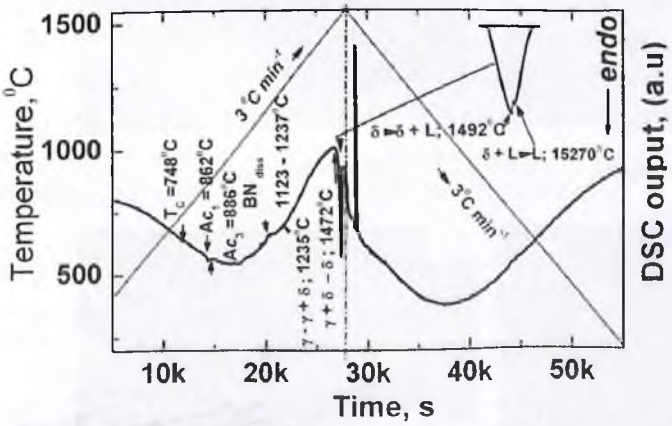

Figue 3 : DSC thermogram illustrating the sequence of phase transformations occurring in P91B up to the melting point under argon atmosphere.

$$\gamma + MX \rightarrow \delta + \gamma + MX \quad \text{..... (1)}$$

The above reaction is followed by the dissolution of MX type of precipitates which was not observed significantly in P91B. Yamada et al. reported 0.05 wt.% of MX type of precipitates, in P91 steel.[12] In earlier section, it was mentioned that nitrogen content was just 20 ppm in P91B steel, therefore MX type of nitrides and carbonitrides would not be formed in large quantity, the dissolution of MX types of precipitate is not accompanied by a sharp thermal arrest. The transformation reaction is as follows,

$$\delta + \gamma + MX \rightarrow \gamma + \delta \quad \text{..... (2)}$$

At this point the $\delta + \gamma$ are in equilibrium and from then onwards austenite slowly dissolves further on increasing the temperature. Thus the transformation of $\delta + \gamma \rightarrow \delta$ phase takes place at 1472°C, which is clearly marked by a sharp inflection point, shown in **Fig. 3**. The phase transformation is followed by the formation of a liquid phase at about 1492°C, subsequently melting occurs according to the peritectic reaction as follows;

$$\text{Liquid} + \delta \rightarrow \text{Liquid} \quad \text{..... (3)}$$

From the DSC trace, one can easily find out delta-ferrite transformation and stability range at high temperature along with other information like transformation temperatures.

3.3 Effect of preheat temperature on heating and cooling curve

Heating and cooling curved obtained during bead-on-plate welding using Tungsten-Rhenium (C-Type) thermocouple on P91B steel and AISI 410 SS plates, at different preheat

temperatures. Typical heating and cooling curve obtained from the weld center line of P91B steel is shown in **Fig. 4**. From the figures it is evident that peak temperature is higher than that of the melting point of the alloy (1527°C). This high peak temperature is super heating occur during welding.

3.4 Microstructure of weldments

3.4.1 Microstructure of modified 9Cr-1Mo steel weldments

Microstructure of P91B and 410 SS weldment prepared in different preheat conditions are shown in **Figs. 5** and **6**, respectively. From the micrographs, it was apparent that the area fraction of delta-ferrite was decreased with increase in preheat temperature. Area fraction of delta-ferrite estimated from the micrographs of P91B and AISI 410 SS weld metal is shown in **Table 3** and **4**. It was also clear that delta-ferrite was more at the interface compared to weld center. Area fraction of delta-ferrite is more in P91B weldment compared to 410 SS weldment, evident from the micrographs, **Figs. 5** and **6**. From **Fig. 5**, it is clear that bead profile did not changed with increase in preheat temperature in P91B. But, it changed in 410 SS with increase in preheat temperature, **Fig. 6**. Change of bead profile will not be discussed in this paper. High magnification images of the weld interface, obtained from the weldments prepared from RT and 200°C preheated condition are shown in **Fig. 7 (a,b)**. The micrographs clearly show that delta-ferrite is more in within the weld bead made at RT as compared to that prepared at preheated condition.

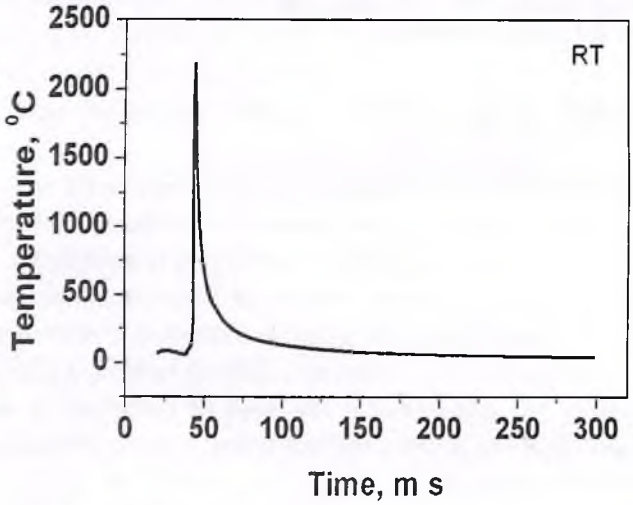

Figure 4 : Heating and cooling curves obtained from the weld metal of P91B steel, bead was made at room temperature

Table 3 : Volume fraction of delta-ferrite weld metal of P91B

Pre heating	Area Fraction of delta-ferrite	
	Weld Interface	Weld center
RT	7.6	6.6
100° C	6.9	5.3
200° C	7.1	4.6
250° C	6.1	4.4

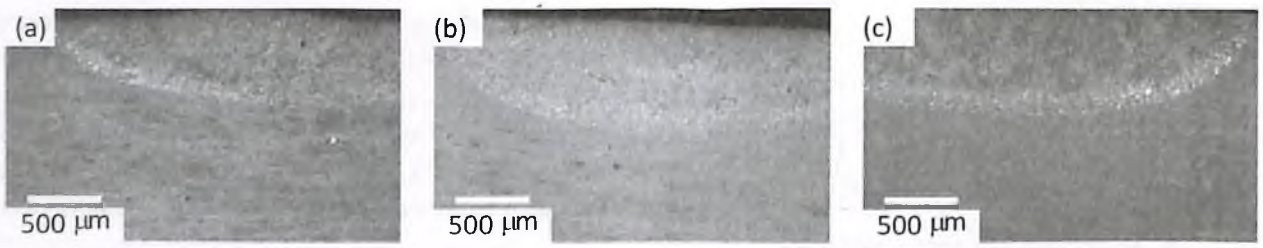

Figure 5 : Microstructure of weld bead for P91B prepared at (a) RT, (b) 100°C and (c) 200°C

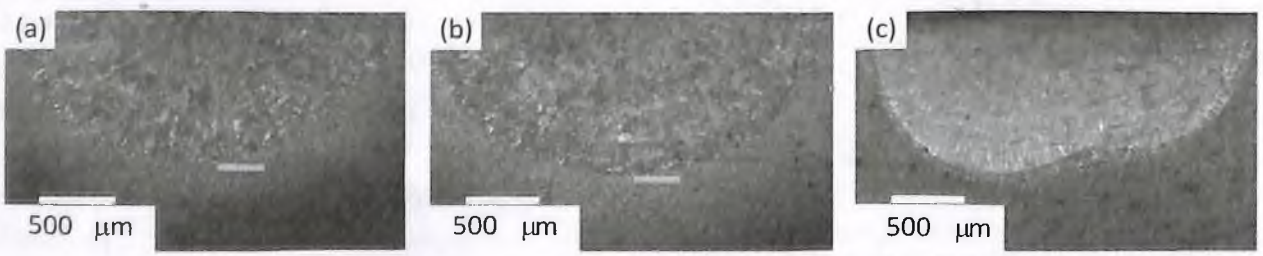

Figure 6 : Microstructure of weld bead for AISI 410 SS prepared at (a) RT, (b) 100°C and © 200°C

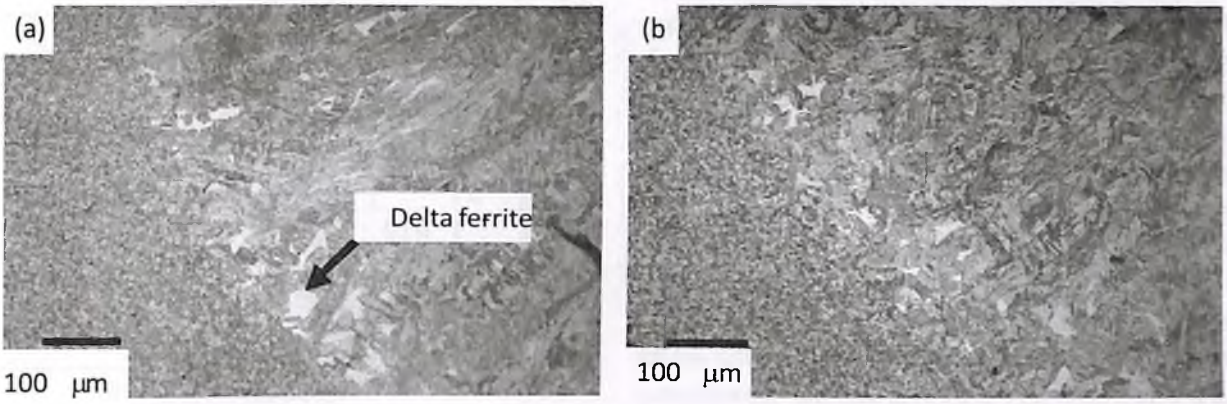

Figure 7 : Microstructure of weld bead for P91B prepared at (a) RT and (b) 200°C

Table 4 : Volume fraction of delta-ferrite weld metal of 410 SS

Pre heating (°C)	Area Fraction of delta-ferrite	
	Weld Interface	Weld center
RT	5.74	5.1
100° C	5.9	4.2
200° C	5.4	5.4
250° C	3.9	5.3

3.4.2 Delta-ferrite prediction

Stability of delta-ferrite at room temperature in high chromium steels can be estimated from empirical formulae available in literature.[13] These formulas describes differences between the weighted effects for the ferrite and austenite forming elements, i.e. the chromium and nickel equivalent values, respectively. Several formulae are available in literature for predicting weld metal microstructure from the chemistry of the metals. In those formulae nickel equivalent can be subtracted from the chromium equivalent describing the relative contributions made from the ferrite and austenite forming elements. The difference is known as ferrite factor. Different formulas used in past to predict delta ferrite are given below:

Schaeffler formula

$$Cr_{eq} = Cr + 1.5Si + Mo + 5V + 0.5Nb + 0.75$$
$$Ni_{eq} = Ni - 0.5Mn - 30C - 30N - 0.3Cu - Co \quad (5)$$

Schneider formula

$$Cr_{eq} = Cr + 2Si + 1.5Mo + 5V + 1.75Nb + 0.75W$$
$$Ni_{eq} = Ni - 0.5Mn - 30C - 25N - 0.3Cu \quad (6)$$

Each formula has been modified subsequently in an attempt to improve the accuracy of the predicted the microstructure. The more recent formulations from Newhouse and Kaltenhuser increase the weighted effect of Mo and Si as ferrite forming elements with respect to former formulae. The Kaltenhauser formula includes the elements Ti and Al but not W, Cu and Co; these are some of the principal elements analysed in this work. **Table 5** shows the results of chromium and nickel equivalent values. Therefore, specific formula may not suite to predict the delta-ferrite in the weld metal of high chromium steels.

Newhouse formula [14]:

$$Cr_{eq} = Cr + 6Si + 4Mo + 11V + 5Nb + 1.5W$$
$$Ni_{eq} = 2Mn + 4Ni + 40C - 30N + 2Co + Cu \quad (7)$$

Kaltenhauser formula [15]:

$$Cr_{eq} = Cr + 6Si + 4Mo + 8Ti + 2Al$$
$$Ni_{eq} = 2Mn + 4Ni + 40(N+C) \quad (8)$$

Table 5 : Chromium and nickel equivalent and formulations according to Schaefler, Schneider, Newhouse and Kaltenhauser

Alloy	Schaeffler		Schneider		Newhouse		Kaltenhauser	
	Cr_{eq}	Ni_{eq}	Cr_{eq}	Ni_{eq}	Cr_{eq}	Ni_{eq}	Cr_{eq}	Ni_{eq}
P91B	11.34	4.81	11.35	4.8	18.04	4.749	15.5	4.77
AISI 410SS	12.56	3.46	12.56	4.8	14.63	5.05	14.63	5.05

Figure 8 shows the weld metal microstructure expected for P91B and 410 SS, according to the Schaeffler diagram. According to Schaeffler diagram, P91B weld metal should have complete martensitic structure whereas 410SS weld metal should have martensite and ferrite microstructure. The results obtained are not reasonable according with the microstrcutral observed for P91B and 410 SS as shown in **Table 3** and **4** as well as in **Fig. 5** and **6**. **Fig. 9** shows the weld metal microstructure expected for P91B and 410 SS weld metal according to the Schneider diagram. According to this diagram both steel should have martensitic microstructure. The results obtained are not reasonable according with the microstrcutral observed for P91B and 410 SS as shown in **Table 4** and **5** as well as in **Fig. 5** and **6**.

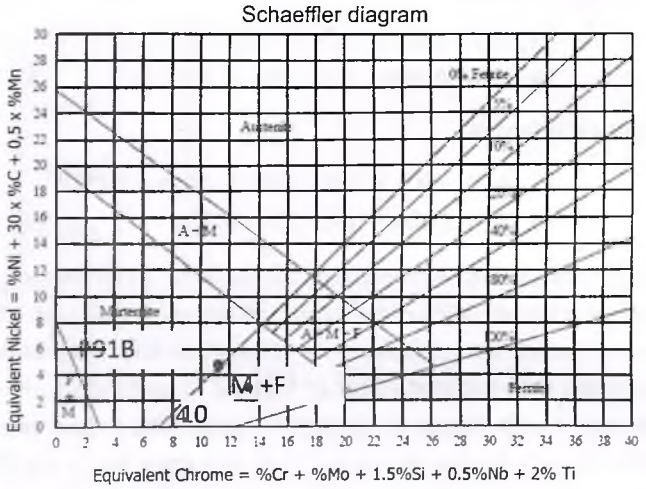

Figure 8 : Weld metal microstructure according to Schneider diagram

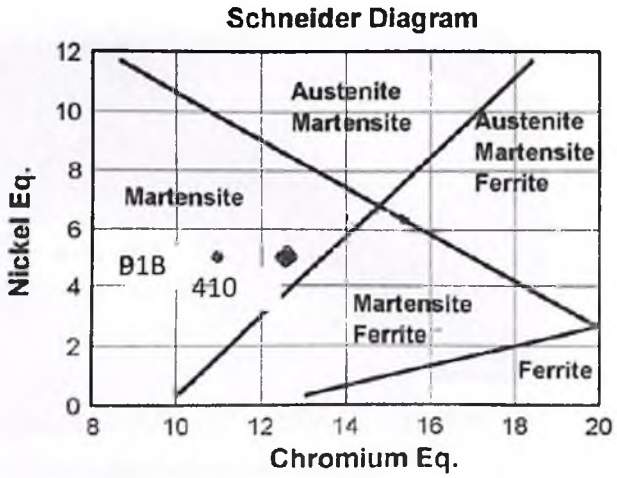

Figure 9 : Weld metal microstructure according to Schneider diagram

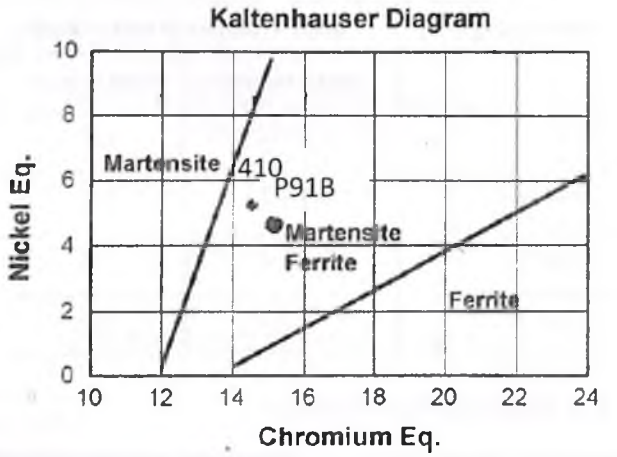

Figure 10 : Weld metal microstructure according to Kaltenhauser diagram

Relatively, new constituent diagram for martensitic and ferritic stainless steel improved version of Schaefer diagram was proposed by Balmforth and Lippold. [16] **Fig. 10** shows the weld metal microstructure expected for P91B and 410 weld metal. It can be seen that the microstructure observed is accordance with that expected by the diagram. It would be therefore appear that the Kaltenhauser formula does adequately predict the behavior of P91B and AISI 410 weld metal.

DISCUSSION

Microstructural observation revealed that base metals microstructure consists of tempered lath martensite, where precipitates decorate the boundaries. Presence of cent percent lath martensite in base metals, suggests that the heat treatment temperature selection was proper. The evolution of delta-ferrite in the weld metal during solidification is discussed as follows. Delta-ferrite stability temperature range is 1235 to 1527°C in P91B steel, obtained from the DSC experiment. During cooling solidification starts at the weld interface in epitaxial manner to minimise surface energy and progress to the weld center. Cooling rate at the weld interface is higher compared to that in the centre of the weld bead. At higher cooling rate, kinetics of delte-ferrite to austenite transformation is sluggish compared to that at lower cooling rate. As a results delta-ferrite is more at the weld interface, **Fig. 5(a-c), 6(a-c)**. In order to understand, why delta ferrite was more in the weld bead, made at different temperatures, portion of the cooling curve from the melting point to the delta-ferrite transformation temperature range is plotted in **Fig. 11(a)**. It may be noted that heating rate has an effect on the transformation temperatures. For the easiness of the discussion, same transformation temperatures were considered on the plot for different cooling curves obtained at different preheat conditions. Using this concept, time spent in

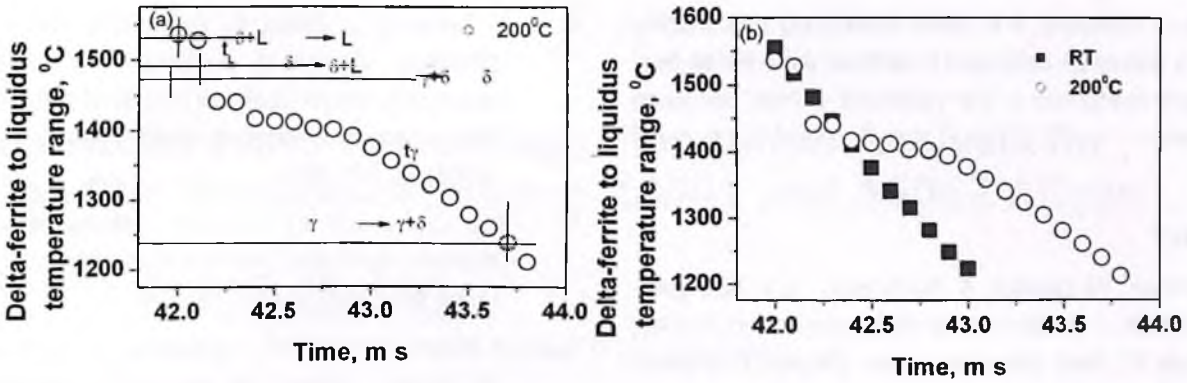

Figure 11 :

the liquid phase as well as in the austenite phase was calculated for delta-ferrite. Time spent in the liquid phase was denoted as t_L and in austenite phase is designated as t_γ. **Fig. 11(b)** shows comparison of cooling curve obtained from RT and 200°C preheat condition. From the curve obtained at RT condition, it is not so clear at what temperature liquid to austenite phase transformation starts but it was clear when curve was obtained at 200°C conditions. t_γ and t_L calculated from the cooling curves in the same way as mention above as shown in **Table 6**. From the table 6, it is evident that time spent in the liquid as well as in austenite phase increases with increase in preheat temperature. But, time spent in the austenite phase was significantly higher than in liquid phase. This suggest, delta ferrite can transformed easily into austenite with increasing preheat temperature. This in turn will bring down the delta-ferrite in the weld metal.

Table 3 : Delta-ferrite stability in liquidius and austenetised temperature range and volume fraction of delta-ferrite for P91B weld metal

Pre heating	Detla-ferrite stability range in liquid	Delta-ferrite stability range in austenite
RT	0.04	0.7
100° C	0.06	0.8
200° C	0.06	1.2
250° C	0.1	1.2

Similarly, delta-ferrite presence in 410SS weld metal can be explained. With progress of cooling, solidification progress to the center of the weld bead. It may be noted that the carbon solubility in delta-ferrite is lower compared to that in austenite phase. As more and more delta-ferrite solidifies in the weld interface, more and more carbon gets rejected into the liquid metal, which enriches the liquid metal. Increase in carbon concentration increases stability of austenite phase, which subsequently transformed into martensite. Hence, less delta-ferrite is observed at the center of the weld bead.

From **Table 5**, it was clear that chromium equivalent is higher for AISI 410SS compared to P91B steel according to Schaeffler and Schneider formulas. It is obvious from the chemical composition analysis, **Table 2**. From equation 5 to 8, it was clear that the coefficient of Mo was high in equation 7 and 8. As results, according to Newhouse and Kaltenhauser equation stability of delta-ferrite would be more in P91B than in 410SS. This is in accordance with the **Fig. 10**, where it was shown that ferrite fraction was more in P91B than in AISI 410SS weld metal. In this paper it was assumed that weld metal composition does not vary significantly from the base metal, hence same composition is used for the analysis. Arivazhagan et al.[17] reported decrease in delta-ferrite in weld metal of RAFM auto-genous bead from 10% to 6% with increase in heat input from 0.81 kJ mm^{-1} to 0.66 kJ mm^{-1}. It may be noted composition of RAFM steel and P91B are similar except Mo in P91B and W in RAFM steel. Decrease in delta ferrite with increase in heat input is attributed to decrease in cooling rate. Authors also reported complete absence of delta-ferrite in the weld metal prepared without any preheating, keeping heat input of 0.66 kJ mm^{-1}. Hence, it is reasonably understood that stability of delta-ferrite at room temperature in high chromium steels depends on many factors other than chemical

composition. Therefore, it is worth mentioning that welding parameters should be optimised to achieve delta-ferrite free, cent percent martensite in the weldment of high chromium ferritic steels.

REFERENCE

1. C. Panait, W. Bendick, A. Fuchsmann, A.-F. Gourgues-Lorenzon, J. Besson, Study of the microstructure of the Grade 91 steel after more than 100,000 h of creep exposure at 600C, Int. J. Pressure Vessels and Pipning 87 (2010) pp. 326-335
2. S.N. Rosenwasser, P. Miller, J.A. Dalessandro, J.M. Rawls, W.E. Toffollo, and W. Chen: J. Nucl. Mater., 85-86 (1979) 177-182
3. K. Kimura, H. Kushima and K. Sawada, Long-term creep deformation property of modified 9Cr-1Mo steel, Mater. Sci. Engg. A 510-511 (2009) pp. 58-63
4. B.J Ganesh, S. Raju, A.K. Rai, E. Mohandas, M. Vijayalakshmi, K.B.S. Rao and Baldev Raj, Differential scanning calorimetry study of diffusional and martensitic phase transformations in some 9wt-% Cr low carbon ferritic steels, Mater. Sci. Tech., 2009
5. H. Schneider, Invetment casting of high-hot strength 12% chrome steel, Foundary Trade J. 108 (1960) pp. 562-563
6. F.B. Pickering, Physical Metallurgy and the Design of steels, Applied Science Publishers, London, UK, 1978, pp. 165-166
7. C.R. Das, S.K. Albert, G M S K Chaitanya, A.K. Bhaduri and T. Jayakumar, Mechanical Properties of Reduced Activation Ferritic Matrtensitic Steel Weldment Prepared by Electron Beam Welding Process, to be communicated
8. V. Knezevic, J. Balun, G. Sauthoff, G. Inden and A. Schneider, Design of martensitic / ferritic heat-resistant steels for application at 650C with supporting thermodynamic modeling, Mater. Sci. Engg. A 477 (2008) pp. 334-343
9. R.J. Castro and J.J. Cadenet, Welding Metallurgy pf stainless steel and Heat-Resisting steels, Cambridge University Press, London, UK, 1968
10. C.R.Das, S.K.Albert, A.K.Bhaduri, G.Srinivasan, B.S.Murty, Effect of prior microstructure on microstructure and mechanical properties of modified 9Cr-1Mo steel weld joints, Materials Science and Engineering A , 477, 1-2, March (2008), 185-192
11. C.R. Das, Ph.D thesis, IIT Madras, 2011
12. Yamada, K., Igarashi, M., Muneki, S. and Abe, F. Effect of heat treatment on precipitation kinetics in high-Cr ferritic steels. ISIJ Int. 42 pp. (2002) 779-784
13. J. Onoro, Martensitic microstructure of 9-12%Cr steels weld metals, J. Mater. Proce. Tech. 180 (2006) pp. 137-142
14. P. Patriarca, et al., United-state advanced materials developmenet program for steam-generators, Nucl. Technol. 28 (1976) pp. 516-536
15. R.H. Kaltenhauser, Improving the engineering properties of ferritic stainless steels, Met. Eng. Q. 11 (2) 1971 pp. 41-47
16. M.C. Balmforth and J.C. Lipold, A preliminary ferritic-martensitic stainless steel constitution diagram, Weld. Res. Sup. (January) 1(1998) pp. 1s-7s
17. B. Arivazhagan, G. Srinivasan, S.K. Albert and A.K. Bhaduri, A study on influence of heat input variation on microstructure of reduced activation ferritic mrtensitic steel weld metal produced by GTAW process, Fusion Engineering and Design 86 (2011) pp. 192-197